A Weighted Range Sensor Matching Algorithm for Mobile Robot Displacement Estimation

Authors

Samuel T. Pfister[†], Kristo L. Kriechbaum[†], Stergios I. Roumeliotis[‡], Joel W. Burdick[†]

[†] Division of Engineering and Applied Science, California Institute of Technology, Pasadena, California 91125, USA. (email:{*sam,klk,jwb*}*@robotics.caltech.edu*). [‡]Department of Computer Science and Engineering, University of Minnesota, Minneapolis, MN 55455 (email: stergios@cs.umn.edu)

Corresponding Author

Samuel T. Pfister

California Institute of Technology,
Mail Code 104-44
Pasadena, California 91125

Phone : 626-395-4165
Fax : 626-583-4963

Email : *sam@robotics.caltech.edu*

Abstract

This paper introduces a new algorithm to estimate a robot's planar displacement by weighted matching of dense two-dimensional range scans. Based on models of expected sensor uncertainty, our algorithm weights the contribution of each scan point to the overall matching error according to its uncertainty. A general maximum likelihood formulation is used to optimally estimate the displacement between two consecutive poses. We develop uncertainty models that account for effects such as measurement noise, sensor incidence angle, and correspondence error. By explicitly modeling these noise sources, we can calculate a more realistic covariance of the displacement estimate than is done in prior work. A realistic covariance estimate is needed when further combining the displacement estimates with odometric and/or inertial measurements within an estimation or localization framework [1]. Experiments using a Nomad 200 mobile robot and a Sick LMS-200 laser range finder illustrate that the method is more accurate than prior techniques, but with comparable computational requirements.

Index Terms

Displacement estimation, mobile robot localization, range sensing, motion from structure, laser scanner, sensor modeling.

Type: Regular Paper

A Weighted Range Sensor Matching Algorithm for Mobile Robot Displacement Estimation

Samuel T. Pfister[†], Kristo L. Kriechbaum[†], Stergios I. Roumeliotis[‡], Joel W. Burdick[†]

***Abstract*— This paper introduces a new algorithm to estimate a robot's planar displacement by weighted matching of dense two-dimensional range scans. Based on models of expected sensor uncertainty, our algorithm weights the contribution of each scan point to the overall matching error according to its uncertainty. A general maximum likelihood formulation is used to optimally estimate the displacement between two consecutive poses. We develop uncertainty models that account for effects such as measurement noise, sensor incidence angle, and correspondence error. By explicitly modeling these noise sources, we can calculate a more realistic covariance of the displacement estimate than is done in prior work. A realistic covariance estimate is needed when further combining the displacement estimates with odometric and/or inertial measurements within an estimation or localization framework [1]. Experiments using a Nomad 200 mobile robot and a Sick LMS-200 laser range finder illustrate that the method is more accurate than prior techniques, but with comparable computational requirements.**

***Index Terms*— Displacement estimation, mobile robot localization, range sensing, motion from structure, laser scanner, sensor modeling.**

I. Introduction and Preliminaries

A robot's ability to determine and maintain knowledge of its absolute position is a basic requirement for long term autonomous navigation and operation. Consequently, the subjects of localization and mapping have justifiably received considerable attention in the last 15 years (e.g., see [2], [3], [4], [5], [6], [7]). Two-dimensional range finders, such as laser range finders [8] or rings of ultrasonic range sensors [9], are often used as a part of many mobile robot localization and mapping procedures. This paper introduces a "weighted" range sensor data matching algorithm to estimate a robot's displacement between the configurations where dense two-dimensional range scans are obtained. This novel algorithm takes into account several important physical phenomena that affect range sensing accuracy, and that have been neglected in prior work. Our experiments (Section VI) show that this algorithm is not only efficient, but appreciably more accurate than non-weighted matching methods, such as that of Ref. [10]. In addition, by computing a more realistic covariance of the displacement estimates, the weighted matching algorithm provides a better basis for fusion of these estimates with odometric and/or inertial measurements [1]. The fused estimates can subsequently support localization and mapping tasks.

[†] Division of Engineering and Applied Science, California Institute of Technology, Pasadena, California 91125, USA. (email:{*sam,klk,jwb*}*@robotics.caltech.edu*). [‡]Department of Computer Science and Engineering, University of Minnesota, Minneapolis, MN 55455 (email: stergios@cs.umn.edu)

To best understand the content of this paper and its contributions, we first describe the basic problem, how our solution differs from previous ones, and the generality of our approach. We focus on mobile robots operating in planar environments. We assume that the robot is equipped with a dense planar range sensor (e.g., a laser range scanner). As discussed in Section II-D, on-board odometry is useful, but not essential.

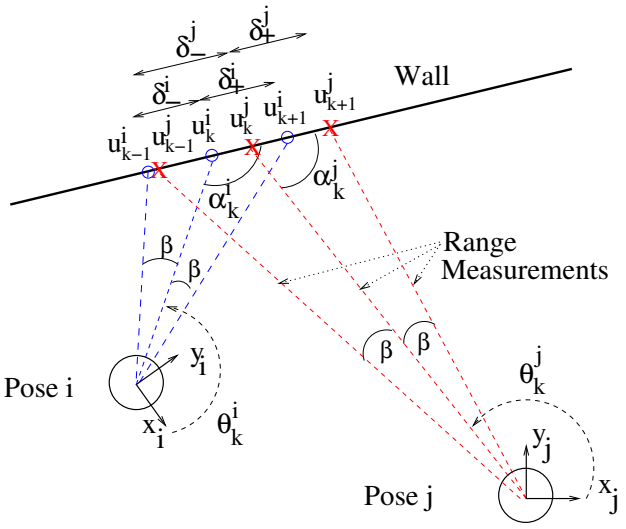

Fig. 1. Geometry of the range sensing process. The robot acquires dense range scans in poses i and j. The circles represent robot position, while the x-y axes denote the robot's body fixed reference frames.

The robot starts at an initial configuration, g_1, and moves through a sequence of configurations, or poses, g_i, $i = 2, \ldots, m$. Here $g_i \in SE(2)$ denotes the robot's position and orientation relative to a fixed reference frame, g_0. We assume that at each pose, the robot measures the range to the boundary of its nearby environment along rays which are separated by a uniform[1] angle, β (see Fig. 1). As described below, we allow for various uncertainties in this range measurement.

Let the set of Cartesian coordinates of the n_i scan points taken in the i^{th} robot pose be denoted by $\{\vec{u}_k^i\}$, $k = 1, \ldots, n_i$. The scan point coordinates are described in the robot's body fixed reference frame. Typically, the Cartesian coordinate of the scan point is derived from range data according to the expression:

$$\vec{u}_k^i = \begin{bmatrix} x_k^i \\ y_k^i \end{bmatrix} = l_k^i \begin{bmatrix} \cos\theta_k^i \\ \sin\theta_k^i \end{bmatrix} \tag{1}$$

where l_k^i is the measured distance to the environment's boundary along the k^{th} measuring ray. The measuring ray is oriented

[1]The extension to non-uniform angle β is straightforward.

in the direction denoted by θ_k^i, where θ_k^i is the angle made by the k^{th} measuring ray with respect to the x-axis of the body fixed reference frame (see Fig. 1).

Our main goal is to accurately estimate the robot's displacement between poses by matching range data obtained in sequential poses. This displacement estimate can be used as the basis for a form of odometry, or fused with conventional odometry and/or inertial measurements to obtain better relative robot pose estimates. These estimates in turn can support localization and mapping procedures. First, assume that the range scans at poses i and j have a sufficient number of corresponding points to be successfully matched (see Section IV). Let $\{\vec{u}_k^i, \vec{u}_k^j\}$ for $k = 1, \ldots, n_{ij}$ be the set of corresponding matched scan point pairs, where n_{ij} is the number of corresponding pairs. From these pairs we first want to estimate the relative displacement between poses i and j: $g_{ij} = g_i^{-1} g_j = (R_{ij}, p_{ij})$ where

$$R_{ij} = \begin{bmatrix} \cos\phi_{ij} & -\sin\phi_{ij} \\ \sin\phi_{ij} & \cos\phi_{ij} \end{bmatrix} \qquad \vec{p}_{ij} = \begin{bmatrix} x_{ij} \\ y_{ij} \end{bmatrix} \tag{2}$$

i.e., the displacement between poses i and j is described by a translation (x_{ij}, y_{ij}) and a rotation, ϕ_{ij}.

We next wish to estimate the covariance, P^{ij}, of the displacement estimate. This covariance has two main uses. First, it reflects the quality of the displacement estimates. Large diagonal elements of the covariance matrix indicate increased uncertainty. Any localization process should be aware of the level of confidence in its computed pose estimates. Second, the covariance is also needed when combining displacement estimates with measurements provided by other sensors. More accurate and realistic estimates of the contributing covariances lead to more accurate overall estimates in a sensor fusion algorithm, such as a Kalman filter.

Our approach differs from prior work in that the contribution of each scan point to the final displacement estimate is individually weighted according to that point's specific uncertainty. The scan point uncertainties are estimated using sensor measurement noise models as well as models of specific geometric issues within the matching process itself. To better understand these issues, examine Fig.s 1 and 2. Fig. 1 depicts the situation when a range sensor (e.g., a laser range finder) samples points on a nearby wall. The boundary points sampled in pose i are indicated by circles, and labeled by $\vec{u}_{k-1}^i$, $\vec{u}_k^i$, and $\vec{u}_{k+1}^i$. The nearby boundary points sampled in pose j are indicated by X's and are labeled by $\vec{u}_{k-1}^j$, $\vec{u}_k^j$, and $\vec{u}_{k+1}^j$. Prior range matching methods (e.g., [11], [12], [13]) have made the simplifying assumption that the range scans of different poses sample the environment's boundary at *exactly* the same points—i.e., point $\vec{u}_k^i$ is assumed to be exactly the same point as $\vec{u}_k^j$, etc. *This assumption is generally not true*. In this paper, we model this *correspondence error* and incorporate this effect into our matching algorithm.

As described in Sections III-A and III-C, the range measurements are corrupted by noise and possibly a bias term that is a function of the range sensing direction, θ_k^i, and the sensor beam's incidence angle, α_k^i (Fig. 1). Figure 2 shows the 95% confidence level ellipses associated with the covariance estimates (calculated using the methods that we will introduce later) of selected data points from an actual laser range scan. Clearly, the wide variation in uncertainties seen in Fig. 2 strongly suggests that not all range data points are of equal precision. Hence, this potentially large variability should be taken into account in the estimation process. While the existence of these uncertainty sources has previously been suggested [14], [8], [13], [15], [16], our algorithm is the first to explicitly model and account for their effects within the estimation process. Some prior works have no explicit noise modeling (e.g. [11]), or apply a uniform uncertainty to all contributing points. The most complete existing methods [14] and [17] employ statistical methods to calculate displacement estimate uncertainty. These methods do not take sensor uncertainty models into account in the displacement estimation process and use an unweighted assumption for the contributing points. Also [14] and [17] do not use any specific sensor noise characteristics as a basis for calculating uncertainty but instead use a numerical sample of perturbations to extract an estimate of covariance. We are able to demonstrate significant improvements over previous unweighted methods by developing physically based uncertainty models for each individual point and incorporating these models in both our displacement estimation process and our covariance calculation.

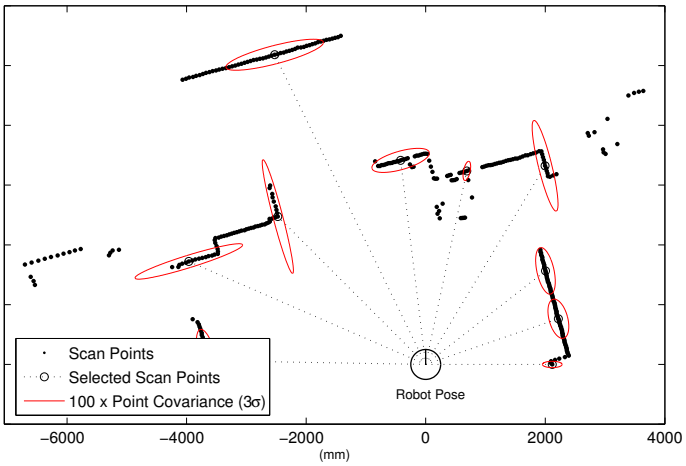

Fig. 2. Representation of the uncertainty of selected range scan points

The basic principle behind our approach generally applies to any case of dense range data, such as sonars, infrareds, cameras, radars etc. The basic weighted matching formulation and its solution given in Section II are independent of any sensor specifics. To use the general results, specific models of sensor uncertainty are needed. We develop these detailed sensor models in Section III. Since some of the assumptions underlying these sensor models are best suited to laser range scanners, the application of our detailed sensor model formulas is best suited to the use of laser scanners in indoor environments, though they can be extended to structured outdoor environments. However, the general approach of Section II should work for other range sensors and other operating environments with reasonable modifications to the sensor models.

This paper is structured as follows. Section II describes a general weighted point feature matching problem and its solution. Section III develops correspondence and range measurement error models. Sections IV and V summarize the

point pairing selection and sensor incidence angle estimation procedures. Experiments in Section VI demonstrate our algorithm's accuracy, robustness, and convergence range. Direct comparisons with previous methods (e.g. [10], [17]) validate the effectiveness of our approach.

II. The Weighted Range Sensor Matching Problem

This section describes a general point feature matching problem and its basic solution.

A. The Measurement Model

Let the sets of Cartesian range scan data points acquired in poses i and j be denoted by the $\{\vec{u}_k^i\}$ and $\{\vec{u}_k^j\}$ respectively. These measurements will be imperfect. Let $\{\vec{r}_k^i\}$ and $\{\vec{r}_k^j\}$ be the "true" Cartesian scan point locations. The measurements can generally be decomposed into the following terms:

$$\begin{aligned} \vec{u}_k^i &= \vec{r}_k^i + \delta\vec{u}_k^i + \vec{b}_k^i \\ \vec{u}_k^j &= \vec{r}_k^j + \delta\vec{u}_k^j + \vec{b}_k^j \end{aligned} \tag{3}$$

where $\delta\vec{u}_k^i$ and $\delta\vec{u}_k^j$ represent noise or uncertainty in the range measurement process, while $\vec{b}_k^i$ and $\vec{b}_k^j$ denote the possible range measurement "bias." These noise and bias terms are discussed in more detail in Sections III-A and III-C. The term $\delta\vec{u}_k$ is generally well modelled by a zero-mean Gaussian noise process. The bias $\vec{b}_k$ is an unknown offset that can be approximated by a term[2] $\vec{o}_k$ corrupted by a zero-mean additive Gaussian noise $\delta\vec{b}_k$ [16]. The covariance of this noise component reflects the level of confidence in the value $\vec{o}_k$. Contingent on this approximation, $\vec{b}_k^i$ and $\vec{b}_k^j$ take the form:

$$\vec{b}_k^i = \vec{o}_k^i + \delta\vec{b}_k^i; \qquad \vec{b}_k^j = \vec{o}_k^j + \delta\vec{b}_k^j. \tag{4}$$

Let $(\vec{u}_k^i, \vec{u}_k^j)$ be points that are deemed to correspond in the range scans at poses i and j. As shown in Fig. 1, these points are not necessarily the same physical point, but the closest corresponding points. Accounting for the fact that scan data is measured in a robot-fixed frame, the error between the two corresponding points is

$$\varepsilon_k^{ij} = \vec{u}_k^i - R_{ij}\vec{u}_k^j - p_{ij} \tag{5}$$

for a given displacement (R_{ij}, p_{ij}) between poses. Substituting Eq. (3) into Eq.(5) results in

$$\varepsilon_k^{ij} = \underbrace{(\vec{r}_k^i - R_{ij}\vec{r}_k^j - p_{ij})}_{(i)} + \underbrace{(\delta\vec{u}_k^i - R_{ij}\delta\vec{u}_k^j)}_{(ii)} + \underbrace{(\vec{b}_k^i - R_{ij}\vec{b}_k^j)}_{(iii)} \tag{6}$$

A relative pose estimation algorithm aims to estimate the displacement $g_{ij} = (R_{ij}, p_{ij})$ that suitably minimizes Eq. (6) over the set of all correspondences. If the dense range scans do sample the exact same boundary points, then $\vec{r}_k^i - R_{ij}\vec{r}_k^j - p_{ij} = 0$ when R_{ij} and p_{ij} assume their proper values. However, $\vec{r}_k^i$ and $\vec{r}_k^j$ generally do not correspond to the same boundary point. Hence, term (i) in Eq. (6) is the *correspondence error*, denoted by c_k^{ij}:

$$c_k^{ij} = \vec{r}_k^i - R_{ij}\vec{r}_k^j - p_{ij}. \tag{7}$$

The matching error ε_k^{ij} for the k^{th} corresponding point is also a function of: (ii) the error due to the measurement process noise, and (iii) the measurement bias error.

For the sake of simplicity, we ignore the bias offsets for now (i.e., we assume that $\vec{b}_k^i = \vec{b}_k^j$=0), but consider their effect again in Section III-C.

B. A General Covariance Model

For subsequent developments, we must derive a generalized expression for the covariance of the measurement errors:

$$\begin{aligned} P_k^{ij} &\triangleq E\left[\varepsilon_k^{ij}(\varepsilon_k^{ij})^T\right] \\ &= E\left[(c_k^{ij} + \delta\vec{u}_k^i - R_{ij}\delta\vec{u}_k^j)(c_k^{ij} + \delta\vec{u}_k^i - R_{ij}\delta\vec{u}_k^j)^T\right] \end{aligned} \tag{8}$$

where $E[\cdot]$ is the expectation operator, and we are ignoring bias effects for now. P_k^{ij} captures the uncertainty in the error between corresponding range point pairs. Because the range measurement noise is assumed to be zero mean, Gaussian, and independent across measurements, $E[\delta\vec{u}_k^i(\delta\vec{u}_k^j)^T] = E[\delta\vec{u}_k^j(\delta\vec{u}_k^i)^T] = 0$. Practically speaking, one would expect that the range measurement noise of the k^{th} scan point in pose i to be uncorrelated to the measurement noise of the k^{th} corresponding range point in pose j. Hence, this is a fine assumption in practice.

The correspondence error, c_k^{ij}, is generally a deterministic variable that is in turn a function of the geometry of the robot's surroundings. However, since we do not assume that the geometry of the environment is known ahead of time, in this work we make a reasonable *probabilistic approximation* to this term which accounts for the fact that the geometry of the surroundings is apriori unknown. In this probabilistic approximating model, the correspondence error and sensor measurement error terms are independent, and therefore $E[c_k^{ij}(\delta\vec{u}_k^i)^T] = E[c_k^{ij}(\delta\vec{u}_k^j)^T] = E[\delta\vec{u}_k^i(c_k^{ij})^T] = E[\delta\vec{u}_k^j(c_k^{ij})^T] = 0$. See Section III-B for a more detailed discussion.

With these assumptions, the covariance of the matching error at the k^{th} point correspondence of poses i and j becomes:

$$\begin{aligned} P_k^{ij} &\triangleq E\left[\varepsilon_k^{ij}(\varepsilon_k^{ij})^T\right] = E\left[c_k^{ij}(c_k^{ij})^T\right] + E\left[\delta\vec{u}_k^i(\delta\vec{u}_k^i)^T\right] \\ &+ R_{ij}E\left[\delta\vec{u}_k^j(\delta\vec{u}_k^j)^T\right]R_{ij}^T \\ &= {}^C P_k^{ij} + {}^N P_k^i + R_{ij}\,{}^N P_k^j R_{ij}^T \qquad (9) \\ &= Q_k^{ij} + R_{ij}S_k^{ij}R_{ij}^T \qquad (10) \end{aligned}$$

[2]The value of $\vec{o}_k$ can be determined by statistical analysis of measurement data.

where

$^{C}P_k^{ij}$ = covariance associated with the approximating correspondence error model

$^{N}P_k^{i}$ = measurement noise covariance of the k^{th} scan point in the i^{th} pose

$^{N}P_k^{j}$ = measurement noise covariance of the k^{th} scan point in the j^{th} pose

$$Q_k^{ij} \triangleq {}^{C}P_k^{ij} + {}^{N}P_k^{i}$$
$$S_k^{ij} \triangleq {}^{N}P_k^{j}.$$

The matrices Q_k^{ij} and S_k^{ij} represent the configuration independent and configuration dependent terms of P_k^{ij}. As shown below, the correspondence errors depend upon the sensor beam's incidence angle. The noise covariances will also generally be a function of the variables θ_k^i, θ_k^j, l_k^i, and l_k^j. Thus, the covariance matrix P_k^{ij} would be expected to vary for each scan point pair (see Figure 2 for an illustration). Hence, it is not suitable to assume, as in prior work (e.g. [17], [10]), that P_k^{ij} is a constant matrix for all scan point pairs.

C. Displacement Estimation via Maximum Likelihood.

We employ a Maximum Likelihood (ML) framework to formulate a general strategy for estimating the robot's displacement from a set of nonuniformly weighted point correspondences. Let $\mathcal{L}(\{\varepsilon_k^{ij}\}|g_{ij})$ denote the *likelihood function* that captures the likelihood of obtaining the set of matching errors $\{\varepsilon_k^{ij}\}$ given a displacement g_{ij}. With the assumptions made above, the $k = 1, \ldots, n_{ij}$ range pair measurements are independent [3] and therefore the likelihood can be written as a product:

$$\mathcal{L}(\{\varepsilon_k^{ij}\}|g_{ij}) = \mathcal{L}(\varepsilon_1^{ij}|g_{ij})\mathcal{L}(\varepsilon_2^{ij}|g_{ij}) \cdots \mathcal{L}(\varepsilon_{n_{ij}}^{ij}|g_{ij}). \quad (11)$$

Recall that the measurement noise is considered to be a zero-mean Gaussian process. Finally, as it is shown in Section III-B, the correspondence noise can be approximated by a zero-mean Gaussian process. Neglecting the bias offset for the moment (see Section III-C), the above assumptions imply that $\mathcal{L}(\{\varepsilon_k^{ij}\}|g_{ij})$ takes the form:

$$\mathcal{L}(\{\varepsilon_k^{ij}\}|g_{ij}) = \prod_{k=1}^{n_{ij}} \frac{e^{-\frac{1}{2}(\varepsilon_k^{ij})^T (P_k^{ij})^{-1} \varepsilon_k^{ij}}}{2\pi\sqrt{\det P_k^{ij}}} = \frac{e^{-M^{ij}}}{D^{ij}} \quad (12)$$

$$\text{where} \quad M^{ij} = \frac{1}{2}\sum_{k=1}^{n_{ij}} (\varepsilon_k^{ij})^T (P_k^{ij})^{-1} \varepsilon_k^{ij} \quad (13)$$

$$D^{ij} = \prod_{k=1}^{n_{ij}} 2\pi\sqrt{\det P_k^{ij}} \quad (14)$$

The optimal displacement estimate is the one that maximizes the value of $\mathcal{L}(\{\varepsilon_k^{ij}\}|g_{ij})$ with respect to displacement. One can use any numerical optimization scheme to obtain this displacement estimate. Note however that maximizing Eq. (12) is equivalent to maximizing the log-likelihood function:

$$ln[\mathcal{L}(\{\varepsilon_k^{ij}\}|g_{ij})] = -M^{ij} - ln(D^{ij}) \quad (15)$$

and from the numerical point of view, it is often preferable to work with the log-likelihood function.

Before discussing the solution to this estimation problem, we first compare this formulation with prior work. Most previous algorithms that take an "unweighted" approach to the displacement estimation problem assume that all of the covariance matrices P_k^{ij} are uniformly the 2×2 identity matrix. Consequently, the maximization of the log-likelihood function reduces to a standard least-squares problem. However, as Fig. 2 and our experiments in Section VI show, such a simplistic covariance approximation for all data points is typically not a theoretically sound one. Ref. [12] allowed for a scalar weighting term, though no guidance was provided on how to select the value of the scalar.

The weighted estimation problem has some inherent structure that leads to efficiency in the maximization procedure. Appendix A proves that the optimal estimate of the robot's translation can be computed using the following closed form expression.

Proposition 1: The weighted scan match translational displacement estimate, $\hat{p}_{ij}$, is:

$$\hat{p}_{ij} = P_{pp} \sum_{k=1}^{n_{ij}} \left((P_k^{ij})^{-1} (\vec{u}_k^i - \hat{R}_{ij}\vec{u}_k^j) \right) \quad (16)$$

where $\hat{R}_{ij} = \hat{R}_{ij}(\hat{\phi}_{ij}^-)$ is the estimated rotational matrix calculated with the current estimate of the orientation displacement $\hat{\phi}_{ij}$, and P_{pp} is given by the formula:

$$P_{pp} = \left(\sum_{k=1}^{n_{ij}} (P_k^{ij})^{-1} \right)^{-1}. \quad (17)$$

There is not an exact closed form expression for estimating the rotational displacement ϕ_{ij}. However, there are two efficient approaches to computing this estimate. In the first approach, the translational estimate of Equation (16) is substituted into Equation (12) (or equivalently, into Equation (15)). Since the resulting expression is a function of the single variable ϕ_{ij}, the estimation procedure reduces to numerical maximization over a single scalar variable ϕ_{ij}, for which there are many efficient algorithms.

Alternatively, one can develop (Appendix B) the following second order iterative solution to the non-linear estimation problem:

Proposition 2: The weighted scan match rotational displacement estimate is updated as $\hat{\phi}_{ij}^+ = \hat{\phi}_{ij}^- + \delta\hat{\phi}_{ij}$, where:

$$\delta\hat{\phi}_{ij} \simeq -\frac{\sum_{i=1}^{n_{ij}} p_k^T (P_k^{ij})^{-1} J q_k}{\sum_{k=1}^{n_{ij}} q_k^T J (P_k^{ij})^{-1} J q_k} \quad (18)$$

where

$$J = \begin{bmatrix} 0 & -1 \\ 1 & 0 \end{bmatrix}, \qquad \begin{aligned} q_k &= \hat{R}_{ij}\vec{u}_k^j \\ p_k &= \vec{u}_k^i - \hat{p}_{ij} - \hat{R}_{ij}\vec{u}_k^j \end{aligned} \quad (19)$$

Using various experimental data, we have found that this approximation agrees with the exact numerical solution up

[3] Possible dependencies of these measurements will be briefly considered in Section III-B. Generally, the only effect that will lead to dependence is possible couplings in the correspondence error that arise if the geometry of the environment is a priori known.

to 5 significant digits. However, it is computationally more efficient to implement.

D. The Algorithm and Its Initial Conditions

Prop.s 1 and 2 suggest an iterative algorithm for estimating displacement. An initial guess $\hat{\phi}_{ij}^{-}$ for ϕ_{ij} is chosen. A translation estimate $\hat{p}_{ij}$ is computed using Prop. 1. This estimate can be used with an exact numerical optimization procedure or with Prop. 2 to update the current rotational estimate $\hat{\phi}_{ij}^{-}$. The improved $\hat{\phi}_{ij}^{+}$ is the basis for the next iteration. The iterations stop when a convergence criterion is reached.

The initial guess, $\hat{\phi}_{ij}^{-}$, will usually be derived from an odometry estimate. However, odometry is not necessary for the method to work. An open loop estimate of the robot's displacement based on the known control inputs that generate the displacement will often provide sufficient accuracy for an initial guess. We show in Section VI-A that the algorithm's performance is not hampered by quite large errors in the initial value of the displacement used as a seed for the algorithm. Note that if odometry does provides the initial guess, there will be no correlation between the estimate arising from our scan matching algorithm and the odometry estimate since the accuracy of the latter is not considered in the estimation process. This simplifies subsequent fusion of these estimates that may be desired for some applications.

We prefer an iterative algorithm for two reasons. First, nonlinear ML problems are suited to iterative computation. Second, the correct correspondence between point pairs cannot be guaranteed in the point correspondence problem (see Section IV). This is especially true in the first few algorithm iterations, where some inaccurate initial pairings are unavoidable. Our iterative approach allows for continual readjustment of the point correspondences as the iterations proceed.

E. Covariance of the Displacement Estimation Error

Letting $\tilde{p}_{ij} = p_{ij} - \hat{p}_{ij}$, $\tilde{\phi}_{ij} = \phi_{ij} - \hat{\phi}_{ij}$ (i.e, $\tilde{p}_{ij}$, $\tilde{\phi}_{ij}$ are translational and the rotational displacement error estimates), a direct calculation yields the following.

Proposition 3: The covariance of the displacement estimate is:

$$P^{ij} = \begin{bmatrix} P_{pp} & P_{p\phi} \\ P_{\phi p} & P_{\phi\phi} \end{bmatrix} = \begin{bmatrix} E\{\tilde{p}_{ij}\tilde{p}_{ij}^T\} & E\{\tilde{p}_{ij}\tilde{\phi}_{ij}^T\} \\ E\{\tilde{\phi}_{ij}\tilde{p}_{ij}^T\} & E\{\tilde{\phi}_{ij}\tilde{\phi}_{ij}^T\} \end{bmatrix}$$

with

$$P_{p\phi} = \frac{1}{r_T}\left(\sum_{k=1}^{n_{ij}}(P_k^{ij})^{-1}\right)^{-1}\sum_{k=1}^{n_{ij}}\left((P_k^{ij})^{-1}Jq_k\right) \quad (20)$$

$$P_{\phi p} = P_{p\phi}^T \quad (21)$$

$$P_{\phi\phi} = \frac{1}{r_T} \quad (22)$$

$$r_T = -\sum_{k=1}^{n_{ij}} q_k^T J(P_k^{ij})^{-1}Jq_k. \quad (23)$$

and P_{pp} is given by Eq. (17).

The proofs for Prop. 3 are given in Appendix C. For a given sensor, one must derive appropriate uncertainty models which are then substituted into the above procedure.

Note 1: The matrix $-J\ (P_k^{ij})^{-1}\ J = \frac{1}{\det(P_k^{ij})}\ P_k^{ij}$ in Eq. (23) is a positive definite matrix and therefore $P_{\phi\phi}$ is a positive number.

Note 2: From Eq.s (22) and (23), we can see that for bounded covariance ($\|(P_k^{ij})^{-1}\| < K\ ,\ 0 < K < \infty$) we have:

$$\lim_{\|\vec{u}_k^j\|\to\infty} P_{\phi\phi} = \lim_{\|q_k\|\to\infty} P_{\phi\phi} = 0.$$

This result leads to the following corollary.

Corollary 4: Matching of distant features (in the limit features at infinite distance from the current location) minimizes the expected error in the orientation displacement estimate. In the limit, the relative orientation error is zero.

Note 3: Since all matrices $P_k^{ij},\ k = 1,\ldots,n_{ij}$, in Eq. (17) are positive definite, the covariance of the translational estimate, P_{pp}, can be written as:

$$\begin{aligned}(P_{pp})^{-1} &= \sum_{k=1}^{n_{ij}}(P_k^{ij})^{-1} > (P_k^{ij})^{-1} \Leftrightarrow \\ P_{pp} &< P_k^{ij}\ ,\ k = 1,\ldots,n_{ij}. \end{aligned} \quad (24)$$

Here we used the notation $X > Y$ to indicate that the difference $X - Y$ is a positive definite matrix. Eq. (24) leads to the following corollary.

Corollary 5: Let $U^{ij} = \min_{k=1,\ldots,n_{ij}} P_k^{ij}$ denote the minimum covariance over all corresponding point pairs. The translational covariance estimate P_{pp} given by Eq. (17) is bounded above by U^{ij}: $P_{pp} < U^{ij}$.

This corollary states that the covariance of the translational estimate will always be less than the best single covariance associated with any corresponding point pair.

III. Scan Matching Error/Noise Models

In order to derive explicit expressions for the covariances of Eq. (10), this section develops models for the errors inherent in the range scan matching process. Most of the models are quite general, though we do make a few assumptions at some points that are most appropriate for laser range scanners.

A. Measurement Process Noise

Many range sensing methods are based on the time of flight (e.g., ultrasound and some laser scanners) or modulation of emitted radiation [16], [8]. The circuits governing these measurement methods are subject to noise. These effects often can be well modelled in a simple way, enabling the simple computation of the covariance contributions ${}^N P_k^i$ and ${}^N P_k^j$. We focus on the computation of ${}^N P_k^i$, as the one for ${}^N P_k^j$ is completely analogous.

Recall the polar representation of scan data, Eq. (1). Let the range measurement, l_k^i, be comprised of the "true" range, L_k^i, and an additive noise term, ε_l: $l_k^i = L_k^i + \varepsilon_l$. The noise ε_l is assumed to be a zero-mean Gaussian random variable with variance σ_l^2 (see e.g., Ref. [16] for justification of this

assumption). Also assume that error or uncertainty exists in the measurement θ_k^i. That is, the actual scan angle differs from the reported or assumed angle of the scan snapshot. Thus, $\theta_k^i = \Theta_k^i + \varepsilon_\theta$, where Θ_k^i is the "true" angle of the k^{th} scan direction, and ε_θ is again a zero-mean Gaussian random variable with variance σ_θ^2. Hence:

$$\vec{r}_k^{\,i} = L_k^i \begin{bmatrix} \cos\Theta_k^i \\ \sin\Theta_k^i \end{bmatrix} = (l_k^i - \varepsilon_l) \begin{bmatrix} \cos(\theta_k^i - \varepsilon_\theta) \\ \sin(\theta_k^i - \varepsilon_\theta) \end{bmatrix}. \quad (25)$$

For small ε_θ, ε_l (which is a good approximation for most laser scanners), expanding Eq. (25) and using the relationship $\delta\vec{u}_k^i = \vec{u}_k^i - \vec{r}_k^{\,i}$ yields

$$\delta\vec{u}_k^i = (l_k^i)\varepsilon_\theta \begin{bmatrix} -\sin\theta_k^i \\ \cos\theta_k^i \end{bmatrix} + \varepsilon_l \begin{bmatrix} \cos\theta_k^i \\ \sin\theta_k^i \end{bmatrix}. \quad (26)$$

Assuming that ε_θ and ε_l are independent, then:

$$\begin{aligned} {}^N P_k^i &= E[\delta\vec{u}_k^i(\delta\vec{u}_k^i)^T] = \frac{(l_k^i)^2\sigma_\theta^2}{2} \begin{bmatrix} 2\sin^2\theta_k^i & -\sin 2\theta_k^i \\ -\sin 2\theta_k^i & 2\cos^2\theta_k^i \end{bmatrix} \\ &+ \frac{\sigma_l^2}{2} \begin{bmatrix} 2\cos^2\theta_k^i & \sin 2\theta_k^i \\ \sin 2\theta_k^i & 2\sin^2\theta_k^i \end{bmatrix}. \quad (27) \end{aligned}$$

The quantities θ_k^i and l_k^i are the ones measured by the laser scanner.

B. Correspondence Error

Here we analyze the correspondence error described in Section II-A. We then derive a probabilistic approximation to this error. Our derivation assumes that the sensor beam strikes an environmental boundary that is locally a straight line segment (Fig. 1). However, this derivation can be extended to other boundary geometries, or it can serve as an excellent tangent approximation for moderately curved boundaries.

We first develop a formula for the maximum possible correspondence error that can occur due to the fact that the exact same boundary points are not sampled in two successive range scans. Consider how nearby scan points will be matched in the vicinity of points $\vec{u}_k^i$ and $\vec{u}_k^j$ in Fig. 1. Let

$$\delta_+^i = ||\vec{u}_{k+1}^i - \vec{u}_k^i||, \quad \delta_-^i = ||\vec{u}_k^i - \vec{u}_{k-1}^i|| \quad (28)$$

denote the distance to the adjacent scan points (from pose i's scan) near the candidate matching point $\vec{u}_k^i$ (see Fig. 1). Similarly, let $\delta_+^j = ||\vec{u}_{k+1}^j - \vec{u}_k^j||$ and $\delta_-^j = ||\vec{u}_k^j - \vec{u}_{k-1}^j||$ denote the distances to the adjacent scan points (from pose j's scan) near the candidate matching point $\vec{u}_k^j$. The maximum distance (or error) between any pair of points that are chosen to be in correspondence will be half of the minimum distance between adjacent scan points. If the error is greater than this value, the point will be matched to another point, or it will not be matched at all. On average, this error will be the minimum of $(\delta_+^i + \delta_-^i)/4$ or $(\delta_+^j + \delta_-^j)/4$. Simple geometric analysis of Fig. 1 shows that

$$\begin{aligned} \frac{\delta_+^i + \delta_-^i}{4} &= \frac{l_k^i \sin\beta}{4}\left[\frac{1}{\sin(\alpha_k^i + \beta)} + \frac{1}{\sin(\alpha_k^i - \beta)}\right] \\ &= \frac{l_k^i \sin\beta}{2}\left[\frac{\sin\alpha_k^i \cos\beta}{\sin^2\alpha_k^i - \sin^2\beta}\right] \quad (29) \end{aligned}$$

Substituting j for i yields the analogous formula for $(\delta_+^j + \delta_-^j)/4$.

We now propose a probabilistic model for the correspondence errors, and develop explicit formulas for its first two moments. For simplicity, and without loss of generality, let the robot be situated so that $\delta_+^i + \delta_-^i < \delta_+^j + \delta_-^j$ (i.e., the correspondence error is defined by pose i). Recall the correspondence error formula of Eq. (6): $c_k^{ij} = \vec{r}_k^{\,i} - R_{ij}\vec{r}_k^{\,j} - p_{ij}$. Letting x be the position along the boundary relative to $\vec{u}_k^i$, the correspondence error is locally a function of x. With no correspondence error, $x = 0$. Since the correspondence error is locally collinear with the boundary's tangent, let $\mu_k^{ij} = c_k^{ij} \cdot t_k$ be the projection of c_k^{ij} onto the unit boundary tangent vector, t_k, at $\vec{u}_k^i$. The vector t_k is positive pointing from $\vec{u}_k^i$ to $\vec{u}_{k+1}^i$. Hence, μ_k^{ij} is a signed quantity, and $c_k^{ij} = \mu_k^{ij} t_k$. The expected value (mean) of the error in the interval $x \in [-\delta_-^i, \delta_+^i]$ is:

$$E[\mu_k^{ij}] = \int_{-\delta_-^i}^{\delta_+^i} \mu_k^{ij}(x)\mathcal{P}(x)dx \quad (30)$$

where $\mathcal{P}(x)$ is the probability that the k^{th} scan point from pose j will be located at x.

We assume that the geometry of the robot's surroundings is not previously known. Therefore, it is not possible to know a priori the probabilistic distribution of the correspondence errors, $\mathcal{P}(x)$. We reasonably assume that $\mathcal{P}(x)$ has an a priori uniform probability. That is, the scan point $\vec{u}_k^j$ that is matched to $\vec{u}_k^i$ could lie anywhere in the interval $[-\delta_-^i, \delta_+^i]$ with no preferred location. Hence $\mathcal{P}(x) = 1/(\delta_+^i + \delta_-^i)$. Realizing that $\mu_k^{ij}(x) = x$ in the interval $[-\delta_-^i, \delta_+^i]$, evaluation of Eq. (30) yields:

$$\begin{aligned} E[\mu_k^{ij}] &= \frac{(\delta_+^i)^2 - (\delta_-^i)^2}{\delta_+^i + \delta_-^i} = \delta_+^i - \delta_-^i \\ &= -2\frac{l_k^i \sin^2\beta\cos\alpha_k^i}{\sin^2\alpha_k^i - \sin^2\beta}. \quad (31) \end{aligned}$$

Note that when the incidence angle is not normal ($\alpha_k^i \neq 90^o$), the mean is non-zero. However, since the mean is proportional to $\sin^2\beta$, this term is negligible when the magnitude of β is small. Hence, we can practically consider the correspondence error to be a zero-mean quantity when β is small (this holds for the experiments described in Section VI). To compute the variance of the correspondence error (using the zero-mean assumption),

$$E[(\mu_k^{ij})^2] = \int_{-\delta_-^i}^{\delta_+^i} \frac{x^2}{\delta_+^i + \delta_-^i}dx = \frac{(\delta_+^i)^3 + (\delta_-^i)^3}{3(\delta_+^i + \delta_-^i)}. \quad (32)$$

Letting $\eta_k^i = \alpha_k^i + \theta_k^i$, and keeping the above results in mind, the covariance of the correspondence error, ${}^C P_k^i$ of Eq. (10), can be found as

$$\begin{aligned} {}^C P_k^i &= E[c_k^{ij}(c_k^{ij})^T] = E[(\mu_k^{ij})^2]t_k t_k^T \quad (33) \\ &= \frac{(\delta_+^i)^3 + (\delta_-^i)^3}{3(\delta_+^i + \delta_-^i)} \begin{bmatrix} \cos^2\eta_k^i & \cos\eta_k^i \sin\eta_k^i \\ \cos\eta_k^i \sin\eta_k^i & \sin^2\eta_k^i \end{bmatrix} \end{aligned}$$

Note that this expression is a function of the sensor beam's incidence angle, α_k^i. In Section V we discuss how to estimate this quantity from the range scan data.

Because we do not want to assume prior knowledge of the environment's geometry, we consider the correspondence errors to be independent. This assumption is conservative in that we do not assume any structure in the environment beyond the immediate geometry of the local point pairs. It would be possible to predict subsequent correspondence errors along a wall (or other regular geometric structure) given the knowledge that the subsequent corresponding point pairs did indeed come from the same exactly straight wall. With a proper line fitting method (e.g., see [18]), the correlations between correspondence errors could be estimated from the line fitting method's uncertainty model[4].

In general, knowing that adjacent corresponding pairs lie along a common wall will significantly reduce the magnitude of Eq. (32), which in turn will lead to lower variances for most of the points along the wall. In this case, the correspondence error variance becomes dominated by the uncertainty in the wall's geometry, which in turn is a function of the line fitting method. These effects can fit easily within our framework if desired, leading to even better displacement estimates and tighter estimate covariances. However, we choose to take a conservative approach where we do not assume that the robot's surrounding geometry is a priori known. Moreover, since the reduction in uncertainty will only occur for points along one line (or other geometric feature), in even modestly complex environments, the amount of precision to be gained by using this approach is unlikely to be worth the complexity of implementing these more advanced methods.

C. Measurement Bias Effects

Range measurement bias is an artifact of some range sensing methods (e.g., see [16]). Since bias models will strongly depend upon the given range sensing method, it is not possible to give a complete summary of bias models for common sensing methods. Instead, we consider a general approach for calculating the effect of bias on the displacement estimate.

To analyze the bias effect, let $\tilde{\varepsilon}_k^{ij} \triangleq \varepsilon_k^{ij} + \tilde{o}_k^{ij}$, where $\tilde{o}_k^{ij} = \vec{o}_k^i - R_{ij}\vec{o}_k^j$ is the total constant bias offset effect at the k^{th} correspondence, and ε_k^{ij} is the previously defined matching error (that ignored the constant bias term). Incorporating the bias offsets, the likelihood function takes the form:

$$\mathcal{L}(\{\tilde{\varepsilon}_k^{ij}\}|g_{ij}) = \prod_{k=1}^{n_{ij}} \frac{e^{-\frac{1}{2}(\tilde{\varepsilon}_k^{ij}-\tilde{o}_k^{ij})^T(\tilde{P}_k^{ij})^{-1}(\tilde{\varepsilon}_k^{ij}-\tilde{o}_k^{ij})}}{2\pi\sqrt{\det \tilde{P}_k^{ij}}} \quad (34)$$

where $\tilde{P}_k^{ij}$ is the covariance matrix with bias uncertainty taken into account:

$$\tilde{P}_k^{ij} = \tilde{Q}_k^{ij} + R_{ij}\tilde{S}_k^{ij}R_{ij}^T \quad (35)$$

where $\tilde{Q}_k^{ij} = Q_k^{ij} + {}^BP_k^i$ and $\tilde{S}_k^{ij} = S_k^{ij} + {}^BP_k^j$, with ${}^BP_k^i = E[\delta\vec{b}_k^i(\delta\vec{b}_k^i)^T]$ and ${}^BP_k^j = E[\delta\vec{b}_k^j(\delta\vec{b}_k^j)^T]$. That is, the covariance formula is updated to include uncertainty in the bias term. To obtain these results, we again assume that the bias noise is uncorrelated with the range measurement noise and the correspondence error (since variance in bias is typically a function of the variability of the surface properties, rather than measurement noise).

Following the derivations that lead to Prop. 1, one can show that the translation estimate in this case is:

$$\hat{p}_{ij} = \tilde{P}_{pp}\sum_{k=1}^{n_{ij}}\left((\tilde{P}_k^{ij})^{-1}(\vec{u}_k^i - \hat{R}_{ij}\vec{u}_k^j + \tilde{o}_k^{ij})\right) \quad (36)$$

Formulas analogous to Eq. (18) can be derived for the orientation estimate as well. The previous covariance formulas take the same structure, with Q_k^{ij} and S_k^{ij} modified to $\tilde{Q}_k^{ij}$ and $\tilde{S}_k^{ij}$ (i.e., to include possible bias uncertainty terms). Clearly, Eq. (36) shows that bias effects can influence the displacement estimate. However, bias models can be used to compensate for bias effects in the estimate.

IV. Selection of point correspondences

The focus of this work is to improve displacement estimation via more accurate considerations of the noise and uncertainty inherent in the estimation process. However, the displacement estimation process clearly depends upon the ability to successfully match corresponding points from range scans taken in adjacent poses. In order to isolate the benefits of our estimation method, we use a very simple "closest-point" rule similar to the one in [10].

Given two scan sets $\{\vec{u}_k^i\}$ and $\{\vec{u}_k^j\}$, the *outliers* are removed in the first step. These are the points visible in one scan, but not in the other (see [10] for details). After removing the outliers, we attempt to find correspondences between scan point pairs in the two poses. For every point in pose i, we search for a corresponding scan point in pose j that satisfies a *range criterion:* the corresponding point must lie within a given distance: $||\vec{u}_k^i - \vec{u}_k^j|| < d$. If no points in pose j satisfy this criterion, then the point is marked as having no correspondence. The parameter d is initially set at a value defined by the error in the initial translation estimate (e.g., the estimated odometry error). Thereafter, to speed convergence, d is monotonically reduced to a value whose order is the maximum point error predicted by our noise model.

It is also possible to establish point correspondences based on a chi-squared analysis of point pairs using the detailed sensor noise models already computed in our method. Though this approach shows promise, in our experimental tests we chose to isolate the estimation benefits of our work. Because unweighted scan-matching methods lack the uncertainty models to perform a chi-squared based point correspondence determination process, we present and compare results using the "closest-point" method for all tests, as this leads to the fairest comparison procedure.

V. Estimating the Incidence Angle

The correspondence error model of Section III-B assumes knowledge of each scan point's incidence angle. While any method of incidence angle estimation can be used, we have chosen a method which estimates the local geometry of the scan points using a Hough transform. The Hough transform

[4]In the case of correspondence error correlations, the likelihood model of Eq. (11) will no longer take a product form. The form of the likelihood model in this case will depend upon the line fitting method.

[19] is a general pattern detection technique which we use to determine an estimate of the supporting line segment about a point. The incidence angle can then be estimated from the configuration of the line segment. In the general Hough transform line finding technique, each scan point $\{x_k, y_k\}$ is transformed into a discretized curve in the Hough space. The transformation is based on the parametrization of a line in polar coordinates with a normal distance from the line to the origin, d_L, and a normal angle, ϕ_L

$$d_L = x_k \sin(\phi_L) + y_k \cos(\phi_L). \tag{37}$$

Values of ϕ_L and d_L are discretized with $\phi_L \in \{0, \pi\}$ and $d_L \in \{-D, D\}$ where D is the maximum sensor distance reading. The Hough space is comprised of a two-dimensional hash table of discrete bins, where each bin corresponds to a single line in the scan point space. For each scan point, the bins in Hough space which correspond to lines passing through that point are incremented. Peaks in the Hough space correspond to lines in the scan data set. As the bins in the Hough space are incremented, we maintain a history of the contributing scan point coordinates in the bin, so that when a peak is determined to represent a line, the contributing set of points can be recovered. The incidence angles can then be estimated for every point in the line.

The algorithm is only precise up to the level of discretization chosen for the line parameters. Both computational complexity and the memory needed for the hash table grow with finer discretization so it is important to establish a reasonable balance between precision and computing resources. For our implementation we found a line angle measurement precise to the nearest degree to be adequate for incidence angle estimation. Discretization in distance was set to 10mm, though this choice of this value is less significant as we are only using the orientation of the fit lines.

The Hough transform is not limited only to straight line detection. It can also be used to detect and fit simple curves such as circles and ellipses and even arbitrary shapes [20]. The tangent vectors to these curves (and subsequently the incidence angle) can then easily be estimated from the transform. For most indoor environments the line fitting method is sufficient to determine incidence angles. More accurate line fitting methods (e.g., [18] and references therein) can be used to get more accurate estimates of incidence angle, but the extra computation is typically not balanced by sufficiently better estimation accuracy.

For points that are not found to be clustered into a line we do not calculate an incidence angle estimate. These points are weighted only according to the computed measurement noises such that the covariance of the matching error at the k^{th} point correspondence of poses i and j from Equation (9) becomes:

$$P_k^{ij} \triangleq {}^N P_k^i + R_{ij}\, {}^N P_k^j R_{ij}^T. \tag{38}$$

where the correspondence covariance estimate ${}^C P_k^{ij}$ has been dropped.

VI. Experiments

We implemented our method on a Nomadics 200 mobile robot equipped with a Sick LMS-200 laser range scanner. This sensor measures the range to points in a plane at every half degree over a 180 degree arc, as seen in Figure 2. For the purpose of comparison, we implemented an unweighted least squares scan matching algorithm analogous to that of Lu and Milios [10], hereafter called the "UWLS." Both the weighted and unweighted estimation algorithms used the same point correspondence algorithm so that the comparison could fairly focus on the relative merits of both estimation schemes. Section VI-A compares the robustness and accuracy of the algorithms in four different environment geometries. Section VI-B compares results from two longer runs. Section VI-C presents the estimated computational costs of the algorithms, while Section VI-D experimentally explores bias compensation. Our experiments used the values $\beta = 0.5^o$, $\sigma_l = 5$ mm, and $\sigma_\theta = 10^{-4}$ radians obtained from the Sick LMS-200 laser specifications.

A. Robustness and Accuracy Comparisons

The experiments reported in this section focus on two aspects of estimation performance: the robustness with respect to errors in the initial displacement estimate that seeds the algorithms' iterations; and the accuracy of the displacement estimates. A more robust algorithm can successfully recover from a wider range of errors in the initial displacement guess. In practice, such errors in the initial displacement estimate come from large odometry errors, or might arise in the absence of odometry when the initial guess is provided by an open loop estimate of the robot's motion response.

To test for robustness, we ran each algorithm through multiple trials with the same pair of scans, each time only perturbing the initial displacement guess. Some initial guesses were sufficiently poor that the algorithm converged to an erroneous solution. An estimate was deemed successful when the true measured displacement lied within the 3σ deviation range as defined by the algorithm's calculated covariance (the UWLS covariance was calculated using the formula given in [17]). The initial displacements we used ranged from 0 to 600 mm at 8 radial directions (every $\pi/4$ radians) at increments of 200 mm in position, and ranged from -0.6 o 0.6 radians in orientation, at increments of 0.02 radians. For each of the 25 discrete initially perturbed positions, we tested 61 initially perturbed orientations to generate 1525 unique initial condition perturbations. These perturbations were added to the true displacement to create initial conditions for the 1525 trials for each algorithm and each environmental condition described below.

We also compare the overall accuracy of each algorithm's displacement measurement. The true displacements are measured by hand with an uncertainty of less than 2mm in displacement and 0.002 radians in orientation. We ran this robustness and accuracy test over four different scan pairs.

Single Pose Test: The first experiment shown in Fig. 3 tests for robustness and accuracy while isolating the effects of our modeling of the point correspondence error (Section III-B). In this test, two scans were taken from the exact same robot pose (i.e., the robot was not moved between scans), with one scan comprised only of the even scan points and the second

Test	Unperturbed Trial: Final Error in Position (mm)		Unperturbed Trial: Final Error in Orientation (mrad)		Percentage of 1525 Perturbed Trials Converged		Converged Trials: Average Error in Position (mm)		Converged Trials: Average Error in Orientation (mrad)	
	Weighted	UWLS	Weighted	UWLS	Weighted	UWLS	Weighted	UWLS	Weighted	UWLS
Fig 3	0.19	1.33	0.23	8.8	91.0%	64.9%	0.63	1.8	0.79	8.6
Fig 4	1.5	3.6	0.43	1.4	82.0%	56.9%	1.8	6.0	0.67	2.6
Fig 5	2.5	9.8	0.57	16.0	95.5%	31.2%	2.5	11.1	0.57	16.0
Fig 6	1.8	4.1	0.0334	0.31	75.1%	3.0%	3.1	14.5	0.0392	0.47

TABLE I

STATISTICS FOR ROBUSTNESS AND ACCURACY COMPARISON TESTS.

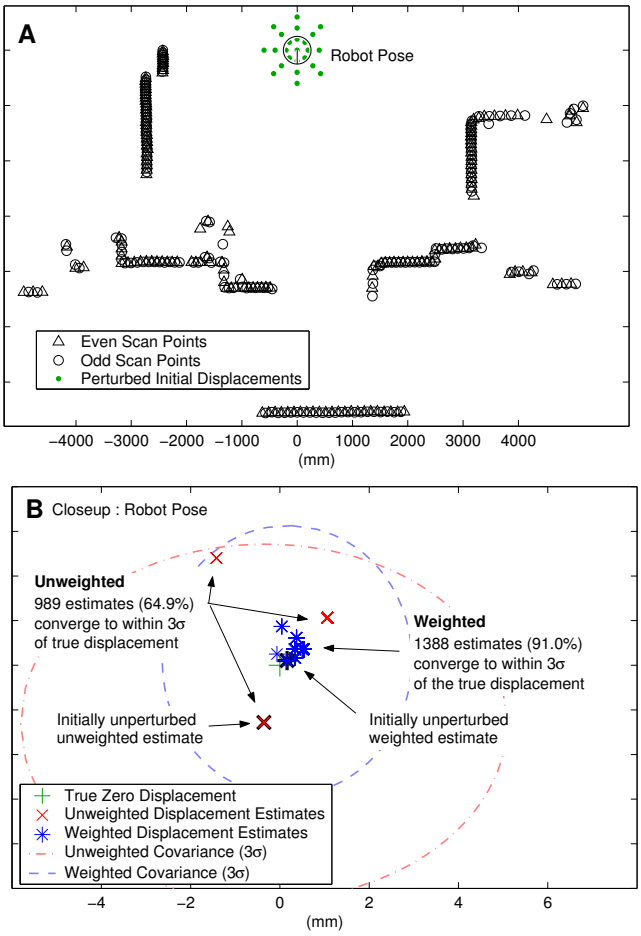

Fig. 3. A) Experiments with initial displacement perturbations between scans taken at a single pose. B) Closeup of robot pose with results.

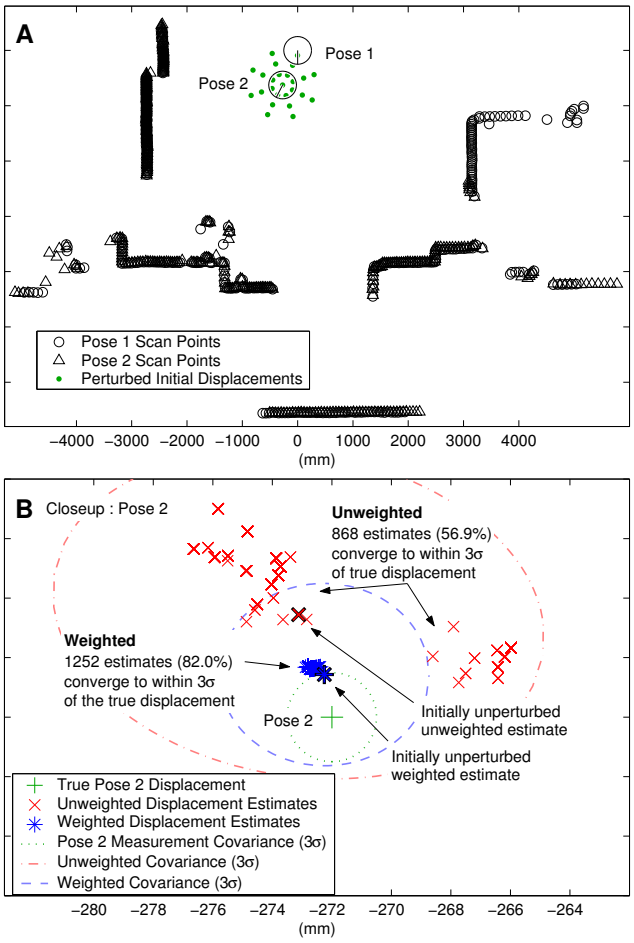

Fig. 4. A) Experiments with initial displacement perturbations between scans taken at different poses. B) Closeup of Pose 2 with results.

scan comprised only of the odd scan points. In this way, correspondence errors are artificially introduced into the two scans.

The two scans and the initially perturbed positions are shown in Fig. 3A. The displacement estimates of the successfully converged estimates are shown in Fig. 3B. The results of the two runs with unperturbed initial guesses are shown with boldfaced markers, along with the 3σ uncertainty boundary of these estimates (shown as dashed ellipses). Of the 1525 runs with initial displacement perturbations our algorithm converged successfully in 91.0% of the cases while the UWLS algorithm was successful in 64.9% of the cases. The average error for successful weighted estimates was 0.63mm and 0.00079 radians while the average error for successful UWLS algorithm estimates was 1.8mm and 0.0086 radians. The error for the case when the initial displacement guess is unperturbed is 0.19mm and 0.00023 radians for our weighted algorithm and 1.33mm and 0.0088 for the UWLS algorithm. Though the true displacement between the poses is exactly zero (since the scans were taken at the same robot pose), due to the even/odd nature of the scans no two corresponding scan points sample the exact boundary points of the environment. The effect of this correspondence error on the UWLS algorithm can be visualized in the presence of three distinct local minima in Fig. 3B. This multi-modal result surrounding the value is often seen in UWLS algorithm robustness test results.

Two Pose Test: Fig. 4 shows results from initial condition robustness testing on two scans taken in our lab with true

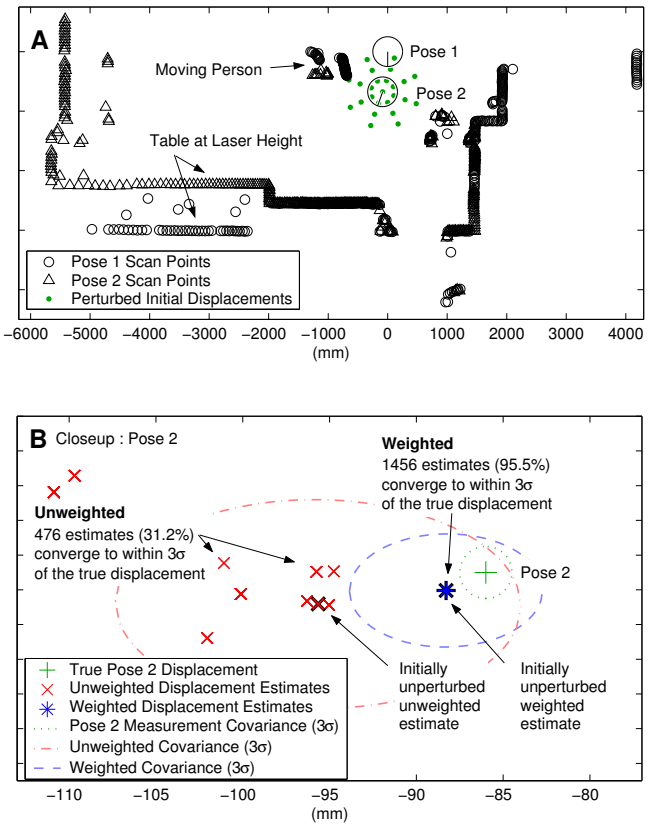

Fig. 5. A) Experiments with initial displacement perturbations in a non-static environment. B) Closeup of Pose 2 with results.

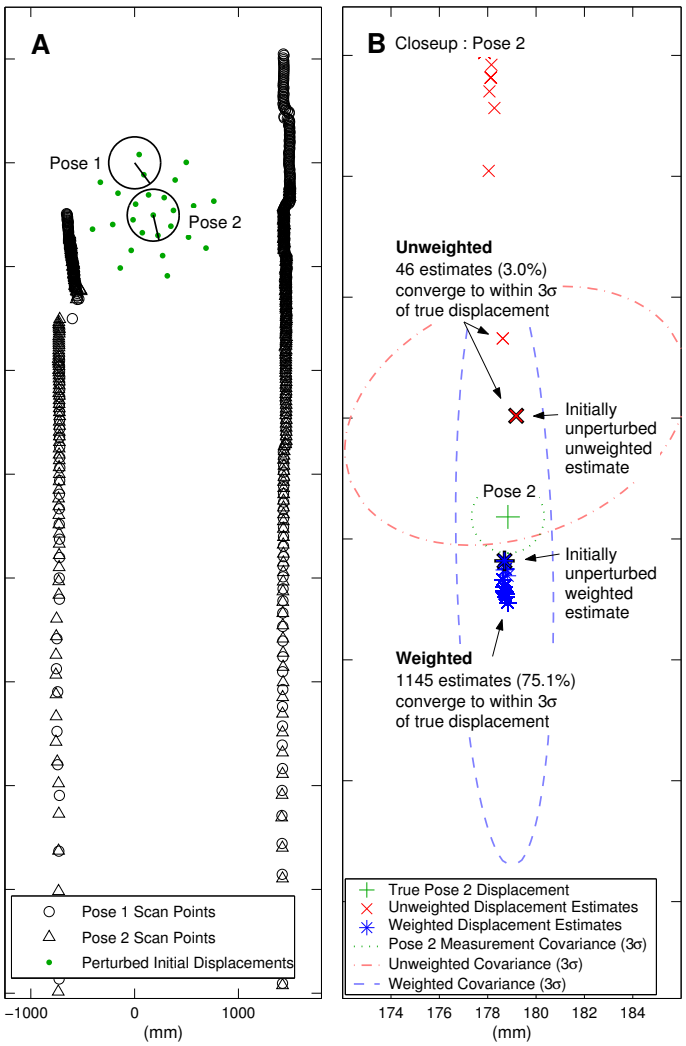

Fig. 6. A) Experiments with initial displacement perturbations in a hallway environment. B) Closeup of Pose 2 with results.

position and orientation displacements of 683mm and 0.467 radians. Fig. 4A shows the robot poses and scans under consideration, as well as the initial perturbed displacement guesses. Fig. 4B shows the results obtained by starting the algorithms from the 1525 different initial displacement perturbations. Our algorithm successfully converged in 82.0% of the cases while the UWLS algorithm was successful in 56.9% of the cases. The average error for successful weighted estimates was 1.8mm and 0.00067 radians while the average error for successful UWLS algorithm estimates was 6.0mm and 0.0026 radians. The error for the case when the initial displacement guess is unperturbed is 1.5mm and 0.00043 radians for our weighted algorithm and 3.6mm and 0.0014 for the UWLS algorithm.

Two Pose Test With IntraScan Changes in the Environment: Fig. 5 shows the results of the same type of testing performed on a pair of scans in which the environment changed between scans. Note that the horizontal double wall on the lower left side of the figure is actually a table at almost exactly laser height. The first scan sampled the wall behind the table while the second scan sampled the front edge of the table due to small changes in floor geometry. The additional nearby obstruction to the left of the robot was caused by a person who moved between the two scans. The range points associated with these non-repeating objects represent 29.2% of the total number of scan points. For the 1525 trials with different initial displacement perturbations, our algorithm was successful in 95.5% of the cases, while the UWLS algorithm was successful in 31.2% of the cases. The average error for successful weighted estimates was 2.5mm and 0.00057 radians while the average error for successful UWLS algorithm estimates was 11.1mm and 0.016 radians. The error for the case when the initial displacement guess is unperturbed is 2.5mm and 0.00057 radians for our weighted algorithm and 9.8mm and 0.016 for the UWLS algorithm. These results show that our method's emphasis on weighting each scan point results in superior robustness to the presence of a significant number of non-corresponding range points.

Two Pose Test In a Hallway: Fig. 6 shows the results of analogous testing done in a nearly symmetrical hallway. In a perfectly symmetrical hallway with no discernible details along the walls, no scan-based algorithm can effectively correct initial displacement errors in the direction along the hallway's main axis. In this test, a single door is open at a slight angle on the left side of the hallway. The presence of this feature allows for possible scan matching convergence. For the set of 1525 initial displacement perturbations, our algorithm successfully converged in 75.1% of the cases while the UWLS algorithm was successful in only 3.0% of the cases.

The average displacement estimate error for the successful weighted estimates was 3.1mm and $3.92 * 10^{-5}$ radians while the average error for successful UWLS algorithm estimates was 14.5mm and 0.00047 radians. The error for the case when the initial displacement guess is unperturbed is 1.8mm and $3.34 * 10^{-5}$ radians for our weighted algorithm and 4.1mm and 0.00031 radians for the UWLS algorithm. In effect, the weighted algorithm better uses the hallway's small non-symmetries to correct the position estimation along the hallway axis. This significantly better performance is primarily due to our approach of modeling the correspondence errors, which discounts the contributions along the hallway's axis (since there is very low certainty in that direction). Instead, the small asymmetries are effectively accentuated. Conversely, in the UWLS algorithm the contributions of the non-symmetries are effectively lost, resulting in very poor correction of position errors along the hallway. The plots of the uncertainty ellipses in Fig. 6B also show how only our weighted algorithm's calculated covariance reflects a greater uncertainty in the direction parallel to the hallway, as would be expected.

B. Multi-Step Runs

The above results showed not only the improvement in robustness of our algorithm over the UWLS algorithm, but also a significant improvement in the overall accuracy of the successful final displacement estimates. This improvement in accuracy is best seen in longer runs with multiple displacement estimates added end to end.

Long Run With Accurate Odometry: Fig. 7 shows a 32.8 meter loop path consisting of 109 poses with the final pose the same as the starting pose. Because of the difficulty of hand measuring each pose we analyze and compare only the initial and final positions. For each step the current and previous scans are processed by each algorithm with odometry supplying the initial guess, and updated displacement and covariance estimates are calculated. In order to maintain statistical independence in our estimates, two scans were taken at each pose, with scan 1 used to match with the pose behind and scan 2 used to match with the pose ahead. In practical applications, such a dual scan procedure would not be necessary, as a Kalman filter could incorporate the scans while accounting for the correlation between successive displacement estimates. However, we do not use that approach here so that we can focus directly on the properties of the displacement estimate, and not worry about the impact of the filter on our results.

In order to close the loop, the second scan taken at the last pose is matched with the first scan taken at the initial pose. Therefore a perfect series of displacement estimates added tip to tail would result in exactly zero overall displacement estimate. For the run shown in Fig. 7, the final odometry error is 1.817 meters and 0.06 radians. The final UWLS algorithm error is 0.271 meters and 0.021 radians while the final weighted algorithm error is 0.043 meters and 0.0029 radians. The ratio of the final translation error to total path length is 5.54% for odometry, 0.82% for the UWLS algorithm, and 0.131% for our weighted algorithm. Perhaps more importantly,

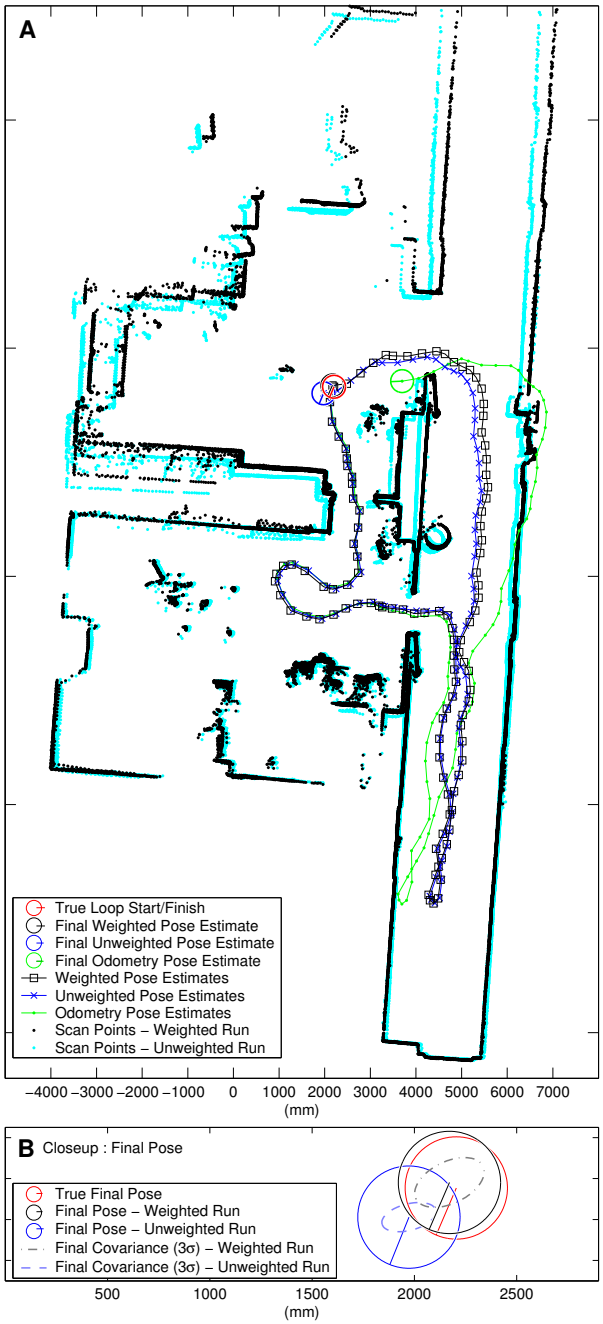

Fig. 7. A) A 109 pose 32.8 meter loop path. B) Closeup of final path poses, shown the covariance estimates of the weighted and unweighted algorithms.

as shown in Fig. 7B, the final covariance calculation for our algorithm clearly encompasses the true final pose within the 3σ bounds, while the covariance calculation of the UWLS algorithm does not.

Long Run With Inaccurate Odometry: This improvement over the UWLS algorithm is even more pronounced in the presence of poor odometry estimates. Fig. 8 shows an actual run where one of the odometry readings was substantially corrupted as the robot rolled over a door jamb when heading into the room in the upper right hand corner of the plot. This path is a 24.2 meter loop consisting of 83 poses with the scans taken and loops closed as in the previous path. For the path shown in Fig. 8 the final odometry error is 1.040 meters

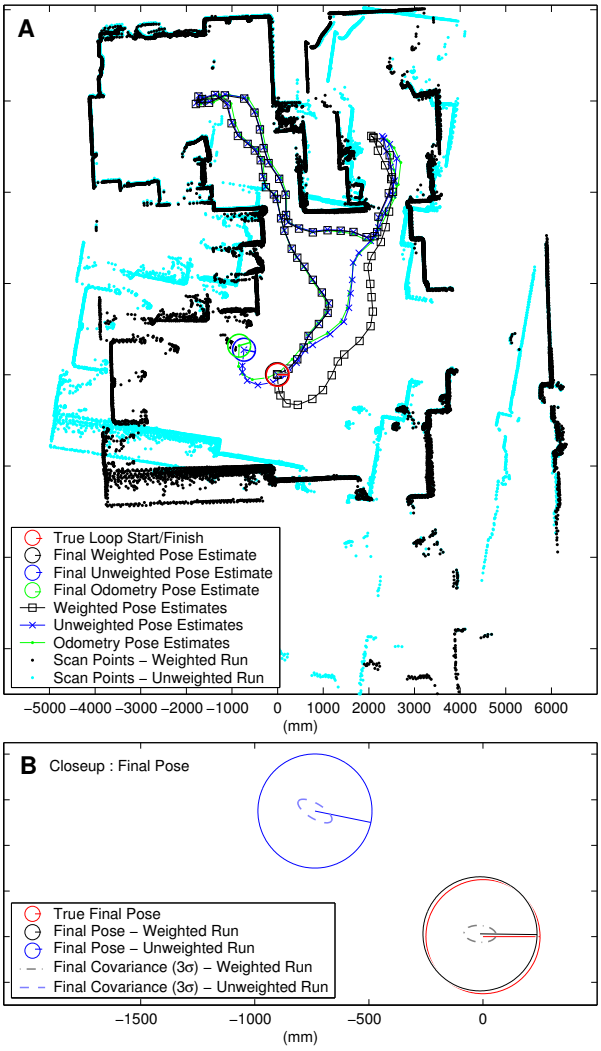

Fig. 8. A) 83 pose 24.2 meter loop. B) Closeup of final loop poses.

and 0.354 radians. The final UWLS algorithm error is 0.919 meters and 0.200 radians while the final weighted algorithm error is 0.018 meters and 0.013 radians. The ratio of the final translation error to total path length is 4.30% for odometry, 3.80% for the UWLS algorithm, and 0.074% for the weighted algorithm.

C. Comparison of Computational Demands

We implemented both algorithms in Matlab and analyzed their computational demands using the Matlab Profiler on a desktop computer with a Pentium 4, 1.80GHz CPU with 512M RAM. Within each iteration, computation is divided between the point correspondence phase (which usually consumes the bulk of the computation) and the estimation phase. The number of iterations required to reach convergence also affects the overall cost of computation.

In the 109 steps of run 1 shown in Fig. 7, the correspondence method used on both algorithms comprises 81.0% of the total UWLS algorithm computation time of 0.112 seconds/iteration and 44.3% of our weighted algorithm computation time of 0.205 seconds/iteration. For the relatively low initial odometry errors in run 1, the UWLS algorithm converges in an average of 12.78 iterations for an average computation time of 1.43 seconds per displacement while our algorithm converges in an average of 10.36 iterations with a total average computation time of 2.12 seconds per pose displacement. For larger initial odometry errors, especially in orientation, the difference in iterations to convergence increases to the point where our weighted algorithm is actually faster than the UWLS algorithm. For the data shown in Fig. 4, when the orientation error is greater than 0.2 radians the UWLS algorithm converges in an average of 42.98 iterations for an average computation time of 4.81 seconds per displacement while our weighted algorithm converges in an average of 22.60 iterations for an average computation time of 4.63 seconds per displacement.

In summary, our experiments show that in real world indoor environments, our method provides significantly greater estimation accuracy and robustness as compared to an unweighted approach without a significant increase in computational cost. Clearly, the computational demands in the estimation phase are larger for our algorithm (as compared to an unweighted algorithm). However, since the computations required by the estimation part of the algorithm account for only a small portion of each iteration, and our algorithm often converges in fewer iterations compared to the UWLS algorithm, the total run time is reduced.

D. Experiments with Bias Compensation

For completeness, we also implemented the bias compensation scheme of Section III-C. In order to implement this scheme, we experimentally determined the laser's range bias in a controlled laboratory setting, and fit a functional relationship to the experimental data. For our experiments, a white paper target was placed at a known distance from the sensor. The center beam of the laser was aligned so as to be normal to the axis of rotation of the target. A total of 100 range measurements were recorded for every 10 degrees of rotation up to 80 degrees from the normal. This process was repeated for nominal ranges of approximately 1.5m, 3m, and 4.2m. Ref. [21] provides a more detailed characterization of this specific laser. The data provided there could be used to build a more detailed model as compared to the one given below.

This experiment showed that the bias for this particular laser sensor is a function of both distance and incidence angle. A function was fit to these data which was then employed to determine the bias, b_r (in mm), in the measurement given the reported distance, r (in mm), from the laser sensor and the angle from normal, α (in radians), from the Hough Transform. Fig. 9 shows both the data collected and the fitting function. The bias function is given by:

$$b_r(r, \alpha) = -14 + 0.004r - 0.035e^{4.9\alpha} \qquad (39)$$

When this bias model was incorporated in the WLSM estimation process, the resulting position estimates were almost unchanged. Over the 21.8 meter, eight-step path described in [22], the incorporation of the bias term resulted in an improvement of only 1.8mm or 0.0082% in the final position estimate. There are two reasons for such a small contribution from the bias term. First, as can be seen in Fig. 9, this laser's

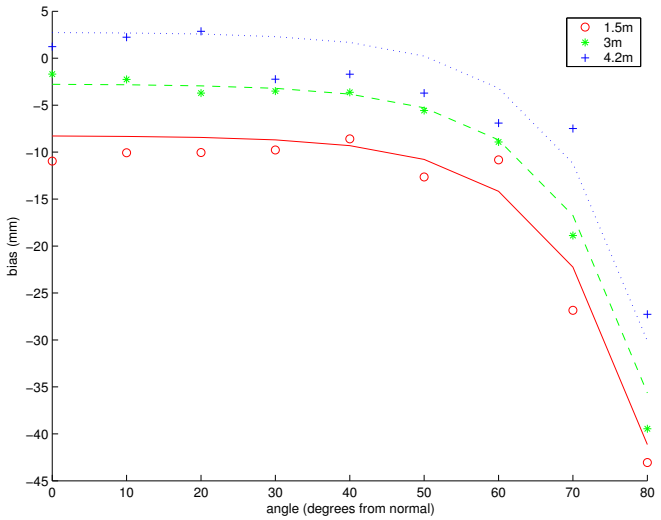

Fig. 9. The bias fit function

bias is quite small and relatively constant (∼1cm) for angles up to 60 degrees from normal. This excellent behavior is certainly due in part to pre-processing that occurs inside the sensor itself. Most of the corresponding points processed by the WLSM algorithm are recorded at angles within the 60^o range. At larger incidence angles, range points are usually sparsely distributed on surfaces far from the sensor and are usually rejected by the matching algorithm since they cannot be paired with the required level of confidence. Even if these points are included, their associated matching covariance is large enough to make their effective contribution negligible. Moreover, symmetries in the environment result in mutual cancellation of the bias effect introduced by points found in opposite directions. Nevertheless we believe that a similar process for estimating the bias can be used and provide improved accuracy in the case of lower quality distance measuring sensors that experience significant bias.

VII. Conclusions

This paper introduced a new method for estimating robot displacement based on dense range measurements. In particular, we investigated the effects of different error and noise sources on the convergence and accuracy properties of these motion from structure algorithms. Our experiments showed that careful attention to the details of error modeling can significantly enhance overall displacement and covariance estimation accuracy.

The first part of the paper gave a general formulation of the displacement estimation problem using weighted point pair correspondences. A general solution to the estimation problem and formulas for the covariance of the displacement estimate were then derived. The application of these results then depends upon explicit error models, and we gave general models for range measurement noise, bias error, and correspondence error. Although parts of this analysis were mainly aimed at planar laser range sensors, the methods can likely be extended to algorithms for non-planar laser scanners [23], [24], where detailed uncertainty modeling has not been considered, and other range sensors such as stereo cameras, radar, ultrasound, etc. Our techniques should also be useful for methods that use both planar laser range finders and cameras to estimate 3-dimensional motion parameters [25], [26]. The specifics of our analysis must be modified to incorporate the appropriate error/noise models for each particular sensor.

The accurate displacement estimates afforded by this method can be fused with odometry estimates [1] to provide better robot localization capability. Similarly, the improved displacement estimation afforded by this method should in the future lead to more accurate map making and localization procedures.

Acknowledgments. This research has was sponsored in part by a National Science Foundation Engineering Research Center grant (NSF9402726) and NSF ERC-CREST partnership award EEC-9730980. We thank Akash Kumar and Ada Yu for helping to implement the UWLS algorithm, and Aisha Chambliss and Derek Jackson for hardware support.

Appendix

A. Weighted Translation Solution

Recall the log-likelihood formula of Eq. (15). Since D^{ij} is independent of x_{ij} and y_{ij}, the necessary condition for an extremal in the log-likelihood function with respect to the variable $p_{ij} = [\ x_{ij}\ y_{ij}\ ]^T$ is:

$$\begin{aligned}
\nabla_{p_{ij}}(M^{ij}) = 0 \quad &\Leftrightarrow \\
\sum_{k=1}^{n_{ij}} \nabla_{p_{ij}} \left((\varepsilon_k^{ij})^T (P_k^{ij})^{-1} \varepsilon_k^{ij} \right) = 0 \quad &\Leftrightarrow \\
2 \sum_{k=1}^{n_{ij}} \left[\left(\nabla_{p_{ij}} (\varepsilon_k^{ij})^T \right) (P_k^{ij})^{-1} \varepsilon_k^{ij} \right] = 0 \quad &\Leftrightarrow \\
-2 \sum_{k=1}^{n_{ij}} \left[I\ (P_k^{ij})^{-1} \varepsilon_k^{ij} \right] = 0 \quad &\Leftrightarrow \\
\sum_{k=1}^{n_{ij}} \left[(P_k^{ij})^{-1} (\vec{u}_k^i - R_{ij} \vec{u}_k^j - p_{ij}) \right] = 0 &
\end{aligned}$$

Rearranging this formula results in Eq. (16).

B. Weighted Rotation Solution

Given an initial estimate of the translational displacement $\hat{p}_{ij}$, the rotational displacement can be derived by maximizing the likelihood function in Eq. (12), or equivalently, the log-likelihood function in Eq. (15) with respect to $\phi_{ij} = \phi$, i.e.

$$\frac{\partial M^{ij}(\phi)}{\partial \phi} = 0. \tag{40}$$

Instead of directly computing the gradient of M^{ij} with respect to ϕ, we calculate it as follows:

$$\frac{\partial M^{ij}(\phi)}{\partial \phi} = \frac{\partial M^{ij}(\hat{\phi} + \delta\phi)}{\partial(\delta\phi)} \frac{\partial(\delta\phi)}{\partial \phi} = \frac{\partial M^{ij}(\delta\phi)}{\partial(\delta\phi)} \tag{41}$$

where we used the relation:

$$\phi = \widehat{\phi} + \delta\phi \Rightarrow \frac{\partial \phi}{\partial(\delta\phi)} = 1\ . \tag{42}$$

Here we derive an exact expression for the quantity M^{ij} as a function of $\delta\phi$. From the Taylor series expansion for the functions $\sin$ and $\cos$ we have:

$$\begin{aligned}\cos\phi &= \cos\widehat{\phi} - \frac{1}{1!}\sin\widehat{\phi}\ \delta\phi - \frac{1}{2!}\cos\widehat{\phi}\ \delta\phi^2 + ... \\ \sin\phi &= \sin\widehat{\phi} + \frac{1}{1!}\cos\widehat{\phi}\ \delta\phi - \frac{1}{2!}\sin\widehat{\phi}\ \delta\phi^2 - ...\end{aligned}$$

Substituting in Eq. (2), the rotational matrix R_{ij} can be written as:

$$R_{ij}(\phi) = \left(I + \frac{1}{1!}J\delta\phi - \frac{1}{2!}I\delta\phi^2 - \frac{1}{3!}J\delta\phi^3 + ...\right)\hat{R}_{ij}(\widehat{\phi})$$

where J is defined in Eq. (19). The error ε_k^{ij} between two corresponding laser points, defined in Eq. (5), can be described as a function of the orientation error $\delta\phi$:

$$\begin{aligned}\varepsilon_k^{ij} &= \vec{u}_k^i - p_{ij} - R_{ij}\vec{u}_k^j \qquad (43)\\ &= \vec{u}_k^i - p_{ij} - \hat{R}_{ij}\vec{u}_k^j - \frac{1}{1!}J\hat{R}_{ij}\vec{u}_k^j\delta\phi \\ &\quad + \frac{1}{2!}\hat{R}_{ij}\vec{u}_k^j\delta\phi^2 + ...\end{aligned}$$

The covariance matrix for the matching error at the k^{th} point correspondence of poses i and j in Eq. (10) can also be described as a function of $\delta\phi$:

$$\begin{aligned}P_k^{ij}(\delta\phi) &= Q_k^{ij} + \widetilde{S}_k^{ij} + (J\widetilde{S}_k^{ij} - \widetilde{S}_k^{ij}J)\delta\phi \\ &\quad - (\widetilde{S}_k^{ij} + J\widetilde{S}_k^{ij}J)\delta\phi^2 - \frac{2}{3}(J\widetilde{S}_k^{ij} - \widetilde{S}_k^{ij}J)\delta\phi^3 \\ &\quad + \frac{1}{3}(\widetilde{S}_k^{ij} + J\widetilde{S}_k^{ij}J)\delta\phi^4 + \quad ... \qquad (44)\end{aligned}$$

where

$$\widetilde{S}_k^{ij} = \hat{R}_{ij}(\hat{\phi})S_k^{ij}\hat{R}_{ij}^T(\hat{\phi}).$$

The inverse $I_k^{ij}(\delta\phi) = (P_k^{ij}(\delta\phi))^{-1}$ of the covariance matrix can be computed using Taylor series expansion as:

$$I_k^{ij}(\delta\phi) = I_k^{ij(0)}(0) + I_k^{ij(1)}(0)\delta\phi + \frac{1}{2!}I_k^{ij(2)}(0)\delta\phi^2 + ... \qquad (45)$$

with

$$I_k^{ij(n)}(0) = \left.\frac{\partial^n(I^{ij}(\delta\phi))}{\partial(\delta\phi)^n}\right|_{\delta\phi=0}$$

where

$$\begin{aligned}I_k^{ij(0)}(0) &= (P_k^{ij}(0))^{-1} = (P_k^{ij})^{-1} = (Q_k^{ij} + \widetilde{S}_k^{ij})^{-1} \\ I_k^{ij(1)}(0) &= -(Q_k^{ij} + \widetilde{S}_k^{ij})^{-1}(J\widetilde{S}_k^{ij} - \widetilde{S}_k^{ij}J)(Q_k^{ij} + \widetilde{S}_k^{ij})^{-1} \\ I_k^{ij(2)}(0) &= 2I_k^{ij(1)}(0)P_k^{ij}(0)I_k^{ij(1)}(0) + 2(\widetilde{S}_k^{ij} + J\widetilde{S}_k^{ij}J).\end{aligned}$$

By substituting from Eq.s (43), (45) to Eq. (13) we have:

$$\begin{aligned}M^{ij} &= \frac{1}{2}\sum_{k=1}^{n_{ij}}\{p_k^T I_k^{ij}(0)p_k \\ &\quad + \left[-2p_k^T I_k^{ij}(0)Jq_k + p_k^T I_k^{ij(1)}(0)p_k\right]\delta\phi \\ &\quad + \Big[p_k^T I_k^{ij}(0)q_k - q_k^T J I_k^{ij}(0)Jq_k \\ &\qquad - 2p_k^T I_k^{ij(1)}(0)Jq_k + \frac{1}{2}p_k^T I_k^{ij(2)}(0)p_k\Big]\delta\phi^2 \\ &\quad + ... \ \} \qquad (46)\end{aligned}$$

where

$$\begin{aligned}p_k &= \vec{u}_k^i - p_{ij} - \hat{R}_{ij}\vec{u}_k^j \qquad (47)\\ q_k &= \hat{R}_{ij}\vec{u}_k^j \qquad (48)\\ \|p_k\| &<< \|q_k\|. \qquad (49)\end{aligned}$$

Note that there has been *no* approximation made up to this point. Eq. (46) is a complete expression of the cost function M_{ij}, expressed as an infinite series of terms polynomial in the orientation estimation error $\delta\phi$. In order to minimize this function, we approximate it after considering a limited number of terms. For small errors in the initial orientation estimate ($\delta\phi < \pi/6$), a second order approximation is sufficient when a large number of point correspondences are available. Higher order approximations are necessary as the number of point correspondences decreases.

By substituting Eq. (46) in Eq. (41) and employing Eq. (49)[5] we derive the expression for the orientation displacement error of Eq. (18).

C. Covariance Estimation

Here we consider the estimation problem where n_{ij} measurements $Z = [Z_1^T \ ... \ Z_{n_{ij}}^T]^T$ (with $Z_k = [(\vec{u}_k^i)^T \ (\vec{u}_k^j)^T]^T$) are processed to derive an estimate of a vector λ of the motion parameters

$$\hat{\lambda} = \begin{bmatrix}\hat{p}_{ij}\\ \hat{\phi}_{ij}\end{bmatrix} = \begin{bmatrix}h_p(Z)\\ h_\phi(Z)\end{bmatrix} = h(Z) \qquad (50)$$

with the expressions for functions h_p and h_ϕ given by Eq.s (16) and (18). A first order approximation of the error in the estimate of the parameter vector $\hat{\lambda}$ is given by:

$$\varepsilon_{\hat{\lambda}} = \nabla_Z^T h(Z)\ \varepsilon_Z = \sum_{k=1}^{n_{ij}}\nabla_{Z_k}^T h(Z_k)\ \varepsilon_{Z_k} \qquad (51)$$

with

$$\nabla_Z^T h(Z) = \begin{bmatrix}\nabla_{Z_1}^T h(Z) & ... & \nabla_{Z_{n_{ij}}}^T h(Z)\end{bmatrix} \qquad (52)$$

and

$$\nabla_{Z_k}^T h(Z) = \begin{bmatrix}\nabla_{Z_k}^T h_p(Z)\\ \nabla_{Z_k}^T h_\phi(Z)\end{bmatrix}. \qquad (53)$$

Note that

$$E\{\varepsilon_{\hat{\lambda}}\} = E\{\nabla_Z^T h(Z)\ \varepsilon_Z\} = \nabla_Z^T h(Z)\ E\{\varepsilon_Z\} = \vec{0}_{3\times 1}.$$

The covariance of the estimate $\widehat{\lambda}$ is:

$$P^{ij} = P_{\widehat{\lambda}} = E\{\varepsilon_{\widehat{\lambda}}\varepsilon_{\widehat{\lambda}}^T\} = \nabla_Z^T h(Z)\ P_Z\ \nabla_Z h^T(Z) \qquad (54)$$

where

$$P_Z = E\{\varepsilon_Z\varepsilon_Z^T\} = \begin{bmatrix}P_{Z_1} & . & 0\\ . & & .\\ 0 & . & P_{Z_{n_{ij}}}\end{bmatrix} \qquad (55)$$

[5] Eq. (49) expresses the fact that the point correspondence errors are very small compared to the distances to these points.

and

$$P_{Z_k} = E\{\varepsilon_{Z_k}\varepsilon_{Z_k}^T\} = E\{\begin{bmatrix} \delta\vec{u}_k^i \\ \delta\vec{u}_k^j \end{bmatrix}\begin{bmatrix} (\delta\vec{u}_k^i)^T & (\delta\vec{u}_k^j)^T \end{bmatrix}\} = \begin{bmatrix} Q_k^{ij} & 0 \\ 0 & S_k^{ij} \end{bmatrix}. \quad (56)$$

Substituting from Eq.s (52), (55) in Eq. (54) yields:

$$P_{\hat{\lambda}} = \sum_{k=1}^{n_{ij}} \nabla_{Z_k}^T h(Z)\ P_{Z_k}\ \nabla_{Z_k} h^T(Z) = \sum_{k=1}^{n_{ij}} \begin{bmatrix} \nabla_{Z_k}^T h_p(Z) \\ \nabla_{Z_k}^T h_\phi(Z) \end{bmatrix} P_{Z_k} \begin{bmatrix} \nabla_{Z_k} h_p^T(Z) & \nabla_{Z_k} h_\phi^T(Z) \end{bmatrix} = \begin{bmatrix} P_{pp} & P_{p\phi} \\ P_{\phi p} & P_{\phi\phi} \end{bmatrix}. \quad (57)$$

For $\xi, \zeta \in \{p, \phi\}$ each of the previous sub-matrices can be written as:

$$P_{\xi\zeta} = \sum_{k=1}^{n_{ij}} \nabla_{Z_k}^T h_\xi(Z) P_{Z_k} \nabla_{Z_k} h_\zeta^T(Z) \quad (58)$$

$$= \sum_{k=1}^{n_{ij}} \Big((\nabla_{\vec{u}_k^i}^T h_\xi)\ Q_k^{ij}\ (\nabla_{\vec{u}_k^i} h_\zeta^T) + (\nabla_{\vec{u}_k^j}^T h_\xi)\ S_k^{ij}\ (\nabla_{\vec{u}_k^j} h_\zeta^T) \Big)$$

where we substituted from Eq. (56) and the relation:

$$\nabla_{Z_k}^T h_\xi(Z) = \begin{bmatrix} \nabla_{\vec{u}_k^i}^T h_\xi(Z) & \nabla_{\vec{u}_k^j}^T h_\xi(Z) \end{bmatrix}.$$

In order to derive the expressions for the covariance sub-matrices we compute the following quantities from Eqs. (16) and (18):

$$\nabla_{\vec{u}_k^i}^T h_p = \left(\sum_{m=1}^{n_{ij}} (P_m^{ij})^{-1} \right)^{-1} (P_k^{ij})^{-1} \quad (59)$$

$$\nabla_{\vec{u}_k^j} h_p = -\left(\sum_{m=1}^{n_{ij}} (P_m^{ij})^{-1} \right)^{-1} (P_k^{ij})^{-1}\ \hat{R}_{ij} \quad (60)$$

$$\nabla_{\vec{u}_k^i}^T h_\phi \simeq -\frac{1}{r_T} q_k J (P_k^{ij})^{-1} \quad (61)$$

$$\nabla_{\vec{u}_k^i}^T h_\phi \simeq -\frac{1}{r_T} q_k J (P_k^{ij})^{-1}\ \hat{R}_{ij} \quad (62)$$

with

$$P_k^{ij} = Q_k^{ij} + \hat{R}_{ij} S_k^{ij} \hat{R}_{ij}^T$$
$$q_k = \hat{R}_{ij} \vec{u}_k^j$$
$$r_T = -\sum_{k=1}^{n_{ij}} q_k^T J (P_k^{ij})^{-1} J q_k\ .$$

In Eq.s (61), (62) we employed the approximation made in Eq. (49). The interested reader is referred to [27] for the details of these derivations.

By substituting Eq.s (59) to (62) in Eq. (58) the sub-matrices of the covariance matrix for the estimated motion vector $\hat{\lambda}^T = [\ \hat{p}_{ij}^T \quad \hat{\phi}_{ij}\ ]$ in Eq. (57) can now be computed. The final expressions are given by Eq.s (17)-(22).

REFERENCES

[1] S. I. Roumeliotis and J. W. Burdick, "Stochastic cloning: A generalized framework for processing relative state measurements," in *Proc. IEEE Int. Conf. on Robotics and Automation*, Washington D.C., May 11-15 2002, pp. 1788–1795.

[2] R. C. Smith and P. Cheeseman, "On the representation and estimation of spatial uncertainty," *Int. J. of Robotics Research*, vol. 5, no. 4, pp. 56–68, 1986.

[3] S. Atiya and G. Hager, "Real-time vision-based robot localization," *IEEE Trans. on Robotics and Automation*, vol. 9, pp. 785–800, Dec. 1993.

[4] J. Leonard and H. Durrant-Whyte, "Mobile robot localization by tracking geometry beacons," *IEEE Trans. on Robotics and Automation*, vol. 7, no. 3, pp. 376–382, June 1991.

[5] J. Neira, J. Tardós, J. Horn, and G. Schmidt, "Fusing Range and Intensity Images for Mobile Robot Localization," *IEEE Trans. on Robotics and Automation*, vol. 15, no. 1, pp. 76–84, Feb. 1999.

[6] S. Roumeliotis and G. Bekey, "Bayesian estimation and Kalman filtering: A unified framework for Mobile Robot Localization," in *Proc. IEEE Int. Conf. on Robotics and Automation*, San Fransisco, CA, Apr. 24-28 2000, pp. 2985–2992.

[7] S. Thrun, D. Fox, and W. Burgard, "A Probabilistic Approach to Concurrent Mapping and Localization for Mobile Robots," *Machine Learning*, vol. 31, pp. 29–53, 1998.

[8] M. Amann, T. Bosch, M. Lescure, R. Myllylä, and M. Rioux, "Laser Ranging: A critical review of usual techniques for distance measurement," *Opt. Eng.*, vol. 40, no. 1, pp. 10–19, Jan. 2001.

[9] J. Crowley, "World modeling and position esitmation for a mobile robot using ultrasonic ranging," in *Proc. IEEE Int. Conf. on Robotics and Automation*, 1989, pp. 674–680.

[10] F. Lu and E. Milios, "Robot Pose Estimation in Unknown Environments by Matching 2D Range Scans," *J. of Intelligent and Robotic Systems*, vol. 20, pp. 249–275, 1997.

[11] J. Gonzalez and R. Gutierrez, "Mobile robot motion estimation from a range scan sequence," in *Proc. IEEE Int. Conf. on Robotics and Automation*, New York, NY, Apr. 20-25 1997, pp. 1034–9.

[12] A. C. Victorino, P. Rives, and J. Borrelly, "A relative motion estimation by combining laser measurement and sensor based control," in *Proc. IEEE Int. Conf. on Robotics and Automation*, Washington D.C., May 11-15 2002, pp. 3924–9.

[13] I. Cox, "Blanche—An Experiment in Guidance and Navigation of an Autonomous Robot Vehicle," *IEEE Trans. on Robotics and Automation*, vol. 2, pp. 193–204, 1991.

[14] O. Bengtsson and A. Baerveldt, "Localization in Changing Environments— Estimation of Covariance Matrix for the IDC algorithm," in *Proc. IEEE/RSJ Int. Conf. on Intelligent Robots and Systems*, Maui, Hawaii, Oct. 2001, pp. 1931–7.

[15] M. Adams, "Lidar Design, Use, and Calibration Concepts for Correct Environmental Detection," *IEEE Trans. Robotics and Automation*, vol. 16, no. 6, pp. 753–761, Dec. 2000.

[16] M. Adams and P. Probert, "The Interpretation of Phase and Intensity Data from AMCW Light Detection Sensor for Reliable Ranging," *Int. J. of Robotics Research*, vol. 15, no. 5, pp. 441–458, Oct. 1996.

[17] F. Lu and E. Milios, "Globally Consistent Range Scan Alignment for Environment Mapping," *Autonomous Robots*, vol. 4, pp. 333–349, 1997.

[18] S. Pfister and J. W. Burdick, "Weighted line fitting algorithms for mobile robot map building and efficient data representation," in *Proc. IEEE Int. Conf. on Robotics and Automation*, Taipei, Taiwan, Sept. 2003.

[19] R. O. Duda and P. E. Hart, "Use of hough transform to detect lines and curves in pictures," *Communications of the ACM*, vol. 15, no. 1, pp. 11–15, 1972.

[20] D. Ballard, "Generalizing the hough transform to detect arbitrary shapes," *Pattern Recognition*, vol. 13, no. 2, pp. 111–122, 1981.

[21] C. Ye and J. Borenstein, "Characterization of a 2-d laser scanner for mobile robot obstacle negotiation," in *Proc. IEEE Int. Conf. on Robotics and Automation*, Washington D.C., May 11-15 2002, pp. 2512–2518.

[22] S. Pfister, K. Kriechbaum, S. Roumeliotis, and J. Burdick, "Weighted range sensor matching algorithms for mobile robot displacement estimation," in *Proc. IEEE Int. Conf. on Robotics and Automation*, Washington, D.C., May 2002.

[23] Y. Liu and M. A. Rodriques, "Accurate registration of structured data using two overlapping range images," in *Proc. IEEE Int. Conf. on Robotics and Automation*, Washington D.C., May 11-15 2002, pp. 2519–24.

[24] A. E. Johnson and A. M. S. Martin, "Motion estimation from laser ranging for autonomous comet landing," in *Proc. IEEE Int. Conf. on*

Robotics and Automation, San Francisco, CA, Apr. 24-28 2000, pp. 1788–1795.

[25] S. Takahashi and B. K. Ghosh, "Motion and shape identification with vision and range," *IEEE Trans. on Robotics and Automation*, vol. 47, no. 8, pp. 1392–6, Aug. 2002.

[26] P. W. Smith, N. Nandhakumar, and C. H. Chien, "Object motion and structure recovery for robotic vision using scanning laser range sensors," *IEEE Trans. on Robotics and Automation*, vol. 13, no. 1, pp. 74–80, Feb. 1997.

[27] S. I. Roumeliotis, "Dense range feature matching: Weighted rotational displacement estimation," C. I. T., Tech. Rep., 2001, http://robotics.caltech.edu/~ stergios/tech_reports/tr_wlsm_orientation.pdf.